PROCEEDINGS, 41st Workshop on Geothermal Reservoir Engineering
Stanford University, Stanford, California, February 22-24, 2016
SGP-TR-209

GIS Methodology for Geothermal Play Fairway Analysis:

Example from the Snake River Plain Volcanic Province

Jacob DeAngelo[1], John W. Shervais[2], Jonathan M. Glen[1], Dennis Nielson[3], Sabodh Garg[4], Patrick Dobson[5], Erika Gasperikova[5], Eric Sonnenthal[5], Charles Visser[6], Lee M. Liberty[7], Drew Siler[5], James P. Evans[2], Sean Santellanes[8]

[1]US Geological Survey, Menlo Park, CA

jdeangelo@usgs.gov, jglen@usgs.gov

[2]Utah State University, Logan, UT

john.shervais@usu.edu, james.evans@usu.edu

[3]DOSECC Exploration Services, Salt Lake City, UT

dnielson@dosecc.com

[4]Leidos, San Diego, CA

sabodh.k.garg@leidos.com

[5]Lawrence Berkeley National Laboratory, Berkeley, CA

pfdobson@lbl.gov, egasperikova@lbl.gov, elsonnenthal@lbl.gov, dlsiler@lbl.gov

[6]National Renewable Energy Laboratory, Boulder, CO

charles.visser@nrel.gov

[7]Boise State University, Boise, ID

lliberty@boisestate.edu

[8]University of Texas, Austin, TX

sean.sant@utexas.edu

Keywords: GIS, Python, Geothermal Play Fairway, Snake River Plain, Common Risk Segment maps

ABSTRACT

Play fairway analysis in geothermal exploration derives from a systematic methodology originally developed within the petroleum industry and is based on a geologic and hydrologic framework of identified geothermal systems. We are tailoring this methodology to study the geothermal resource potential of the Snake River Plain and surrounding region. This project has contributed to the success of this approach by cataloging the critical elements controlling exploitable hydrothermal systems, establishing risk matrices that evaluate these elements in terms of both probability of success and level of knowledge, and building automated tools to process results. ArcGIS was used to compile a range of different data types, which we refer to as 'elements' (e.g., faults, vents, heatflow…), with distinct characteristics and confidence values.

Raw data for each element were transformed into data layers with a common format. Because different data types have different uncertainties, each evidence layer had an accompanying confidence layer, which reflects spatial variations in these uncertainties. Risk maps represent the product of evidence and confidence layers, and are the basic building blocks used to construct Common Risk Segment (CRS) maps for heat, permeability, and seal. CRS maps quantify the variable risk associated with each of these critical components. In a final step, the three CRS maps were combined into a Composite Common Risk Segment (CCRS) map for analysis that reveals favorable areas for geothermal exploration.

Python scripts were developed to automate data processing and to enhance the flexibility of the data analysis. Python scripting provided the structure that makes a custom workflow possible. Nearly every tool available in the ArcGIS ArcToolbox can be executed using commands in the Python programming language. This enabled the construction of a group of tools that could automate most of the processing for the project. Currently, our tools are repeatable, scalable, modifiable, and transferrable, allowing us to automate the task of data analysis and the production of CRS and CCRS maps. Our ultimate goal is to produce a toolkit that can be imported into ArcGIS and applied to any geothermal play type, with fully tunable parameters that will allow for the production of multiple versions of the CRS and CCRS maps in order to better test for sensitivity and to validate results.

1. INTRODUCTION

This work was undertaken as part of an effort to assess undiscovered geothermal resources across the Snake River Plain and surrounding regions (Fig. 1). The project scope and findings are presented in a companion paper at this meeting (*Shervais et al., 2016a*), while this paper is devoted to describing the study's methodology. Play Fairway Analysis estimates the favorability for a resource's presence over an area by identifying the main factors, or *elements* responsible for their occurrence, creating *Common Risk Segment (CRS)* maps that quantify those *components*, and then combining those maps into a final *Composite Common Risk Segment (CCRS)* map of the *components* which will indicate overall favorability. In our attempt to estimate geothermal favorability in the Snake River Plain volcanic province, we looked at *permeability*, *heat source*, and *seal* as the primary *components*. CRS maps for a *component* were created by combining data from all of the *elements* contributing to that *component*. For example, the CRS map for *permeability* was created by combining data about mapped faults and deep structures inferred from geophysics. The CRS map for *heat source* was created by combining regional heat flow, vents, helium isotope ratios, calculated multicomponent equilibrium reservoir temperatures, and measured groundwater temperatures. The CRS map for *seal* was made by combining data reflecting the extent of impermeable lake sediments and regional aquifers with a hydrothermally altered clay seal.

2. APPROACH

What follows is a description of how the *elements* are processed, how they are combined to generate CRS maps, and how CRS maps are combined to generate the CCRS map.

2.1 Processing of Elements

For each of the CRS maps, r*aw data* for every *element* in the study were transformed into surfaces covering the entire study area. For each *element*, we produced a surface showing the magnitude of the transformed *data layer* (the *evidence layer*) as well as a surface showing the uncertainty associated with that magnitude (the *confidence layer*). The product of the *evidence layer* and its *confidence layer* is the *risk layer* for that *element*. *Risk layers* from all of the *elements* used to characterize a *component* are used in creating that *component's* CRS map.

Different processing techniques were applied to the different data types. Processing *data layers* into *evidence layers* involved either *density functions* to calculate the density distribution of an attribute (e.g., volcanic vent or fault segment) or *interpolation*, to calculate a continuous surface from point data (e.g., heat flow, groundwater temperatures). *Density functions* are used for data that are discontinuous by nature, and where the geographic location of that data is important. *Interpolation* is used for data that are by nature continuous, but which can only be sampled at specific points.

Kernel Density Functions assess data density (e.g., vents, fault segments) by counting all instances of a data point within a specified radius of a single point and dividing by the area of the search radius. This density is then distributed from a maximum at the location of the data point to zero at the full radius of the search area using a quadratic function. Data points may be weighted prior to counting. For example, fault segments are weighted by both dilation tendency and slip tendency on a scale from zero to 1.0, as determined by the 3DStress software *(Morris et al., 1996, Ferrill et al., 1999)*.

Empirical Bayesian Kriging (EBK) is an iterative geostatistical *interpolation* method that uses an intrinsic random function as the kriging model, taking into account uncertainties in estimating the semivariogram. Standard errors of prediction are more accurate than other kriging methods, and the results are more accurate for small datasets than other kriging methods *(ESRI ArcGIS Geostatistical Wizard)*. Our standard method for *interpolation* is *Empirical Bayesian Kriging*, a geostatistical process that produces an estimate of the value of a property at each point and a standard error surface that quantifies the uncertainty.

Nearly every tool available in the ArcGIS ArcToolbox can be executed using commands in the Python programming language. This allowed us to create a group of tools that could automate most of the processing for the project. *Raw data* sets had to be manually transformed into *data layers* with a common format before *evidence layers* were processed in the Python script. All *raw data* were processed into ArcGIS shapefiles with a custom projection that maintains area in meters. Interpolated surfaces were created manually for several elements using ArcGIS Geostatistical Wizard. All other work was performed by our Python script.

A raster surface was used in the script to define the study area and the cell size of the project and all further processing was done at the same extent and resolution. All surfaces created in the course of later processing calculated up to the extent of the boundary and their cell centers were in the exact same location. Because every raster surface could be made to line up perfectly, a master point file was created from the study area raster to keep track of every parameter for each cell in the study area. By the end of processing, for every cell in the study area, this point file contained every evidence, confidence, and risk value for every *element* as well as the CRS and CCRS values. All of the calculations were performed on this shapefile and all of the resulting surfaces were converted into surfaces from this point file. All of the modules that process the various *elements* add to this master point file.

In order to create a CRS map, the *risk maps* of the different *elements* are weighted relative to each other before being combined. We refer to these weights between *elements* in the CRS as *intra-CRS weights*. They are specified in the scripting as a list of integers, for example we weighted the *elements* used in the *heat source* CRS map with the following list: [30, 55, 5, 5, 5]. The values are relative only to each other because each CRS map will be normalized before *inter-CRS* weights are applied to them to create the CCRS map. The data from each *element's risk layer* is normalized prior to the application of *intra-CRS weights* so that the different *elements* are of equal value prior to weighting.

Our study used a *knowledge-driven* approach in establishing weights and confidence values. *Knowledge-driven* approaches estimate weight values on the basis of expert opinion while *data-driven* approaches establish weights by use of statistical relationships between elements and known occurrences of the phenomenon being modeled *(Bonham-Carter, 1994)*.

2.2 Permeability

2.2.1 Evidence layers

Four *elements* were examined in constructing the *permeability* CRS map. Mapped faults were assessed along with three sets of lineations interpreted from geophysics: mid-depth gravity, deep gravity, and magnetics. These lineations reflect major lateral contrasts in density and magnetic properties that reveal likely structural features (e.g., faults or contacts) in the subsurface that can provide pathway for fluid flow (e.g., Shervais et al., 2014). Mapped fault data came from the USGS Quaternary fault database *(Machette et al., 2003)* and Idaho Geological Survey data *(Ludington et al., 2005)*. Geophysical data were compiled from a variety of sources *(Bankey et al., 1999; Glen, 2016; McCafferty et al., 1999)*.

Before going into the script, line segments were given a value for both dilation tendency and slip tendency, as determined by the 3DStress software, on a scale from zero to 1.0. A fault segment's tendency to dilate or slip can indicate that it is critically stressed and is therefore more likely to act as a fluid flow conduit and facilitate permeability (Sibson, 1994; Ferrill et al., 1999; Morris et al., 1996). For each *element*, two kernel density surfaces were created, one weighted by dilation tendency and the other by slip tendency (Fig. 1). The values from these surfaces were written to the master point file and a new data column was created with normalized values. These normalized values represent the eight *evidence layers* used for *permeability*.

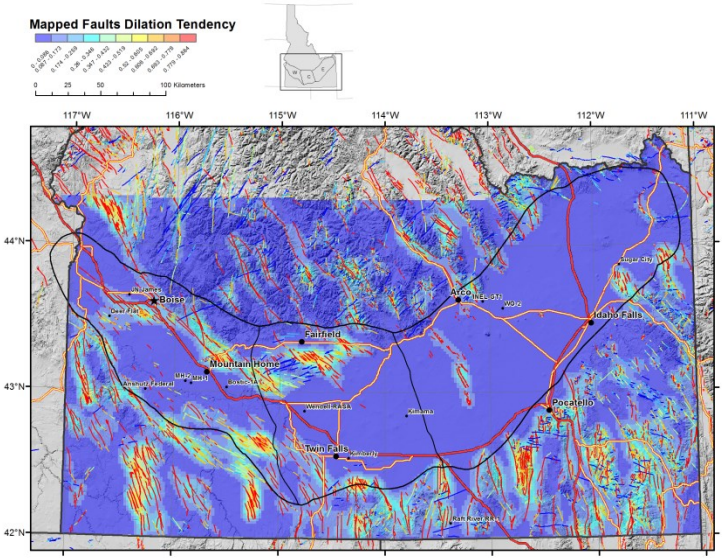

Figure 1. Kernel density surface of mapped faults weighted by dilation tendency. Surface values and faults with warmer colors indicate greater dilation tendency (increased permeability). Similar surfaces were created for magnetic, mid gravity, and deep gravity lineations for both dilation tendency and slip tendency. The geographic extent of our study area coincides with the extent of the colored surface.

2.2.2 Confidence Layers

Three different *confidence layers* were used for the four *elements* examined for *permeability*. The two *elements* derived from gravity both used the same *confidence layer* and weights. *Confidence layers* represent the level of uncertainty in the original measurements. *Confidence layers* for mapped faults and magnetics were polygons covering the entire study area. Each had geographic zones identified with integers from highest to lowest confidence. In our script, we had a list of weights for each *confidence layer* that corresponded to the integer values (Fig. 2-A, B). A new column was written to the master point file with the weight values from our weights lists. The *confidence layer* for both gravity layers was constructed by creating a surface that showed the distance to the nearest gravity station and using distances set in a list to classify break points for assigning weights that were stored in another list (Fig. 2-C).

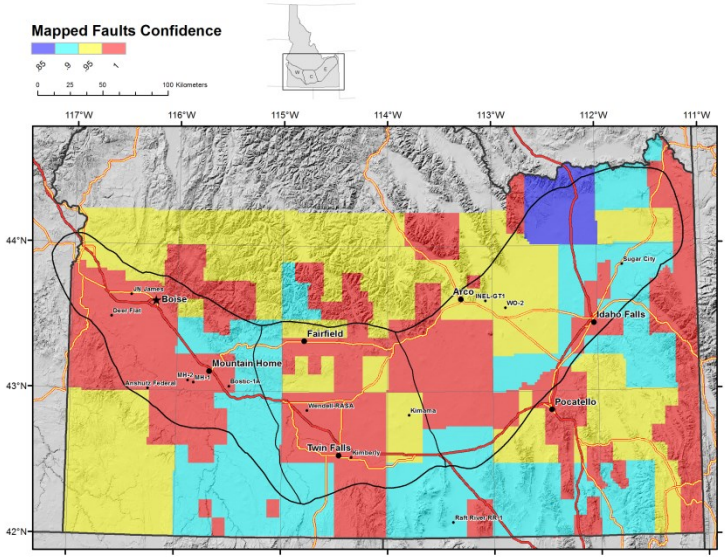

Figure 2-A. Confidence for mapped faults determined by the scale of geologic mapping in the area showing level of uncertainty in original measurements.

2.2.3 Permeability risk layers and CRS

The risk values for each *element* were calculated in the master point file by multiplying the evidence and confidence values. Next, the CRS value for *permeability* was calculated by multiplying each risk *element* by its weight from the list of *intra-CRS weights* for *permeability*, adding those products together, and normalizing the data. These values for the *permeability* CRS were output to a raster surface for display (Fig. 3).

2.3 Heat Source

Five *elements* were examined in constructing the *heat source* CRS map: Vents, heat flow, helium, multicomponent equilibrium reservoir temperatures, and groundwater temperatures.

2.3.1 Volcanic vents

Volcanic vents were brought in as point locations *(Shervais at al., 2015; Shervais at al., 2016b)*. Before processing, each vent was assigned integer values describing its size and age in order of relevance. These size and age categories corresponded to lists of weights in our script for size and age. For each vent, the weight value from its age category was multiplied by the weight value from its size category and stored as the vent's weight. For example, if a vent was assigned the second highest class for size and the highest value for age, the vent's weight would be calculated as the product of the second weight value in the list for size and the first weight value in the list for age. This weight value was then used in a weighted kernel density surface to create the *evidence layer* (Fig. 4). The values from the *evidence layer* were copied to the master point file and a new column was added with normalized values. No *confidence layer* was used with young vents because it is believed that all vents have been identified (older vents may be obscured by younger flows). The normalized *evidence layer* therefore serves as the *risk layer* for vents.

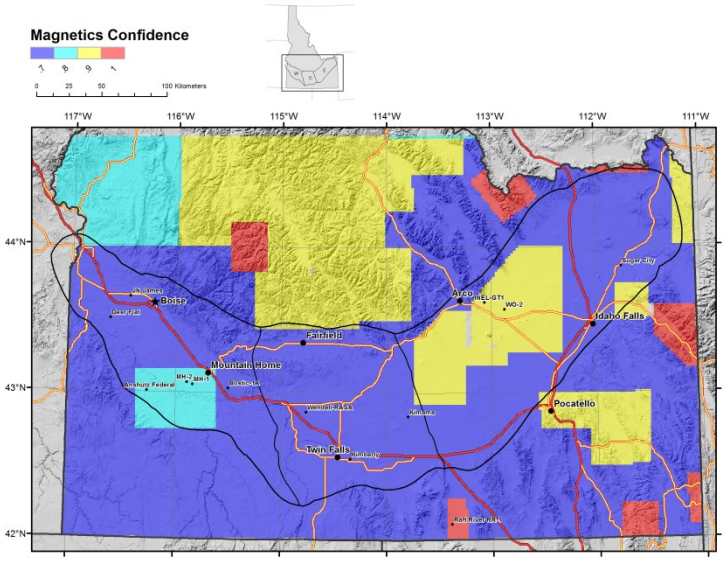

Figure 2-B. Confidence for magnetics determined by the flight specifications of aeromagnetic surveys showing level of uncertainty in original measurements (line spacing and elevation above terrain).

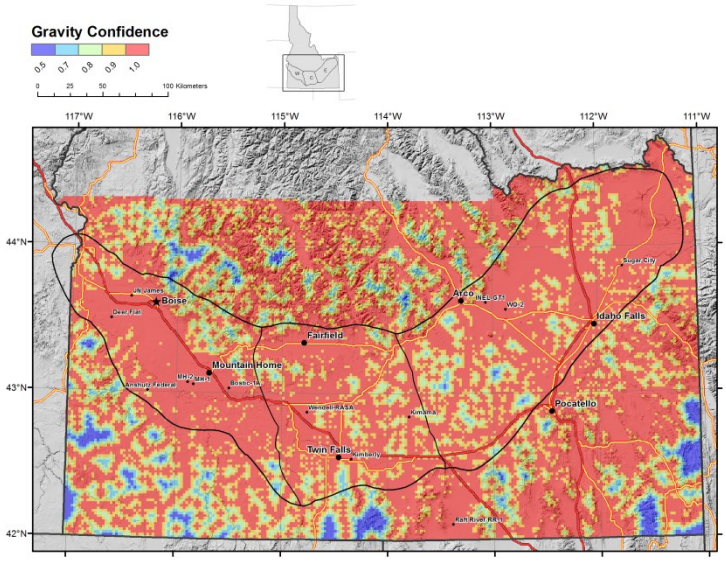

Figure 2-C. Confidence for gravity showing level of uncertainty in original measurements determined by distance to nearest gravity station.

2.3.2 Heat flow

Heat flow data were compiled from USGS and Southern Methodist University (SMU) Geothermal Lab databases *(e.g., Williams and DeAngelo, 2008; 2011; Blackwell et al., 1989; Blackwell and Richards, 2004),* These data were originally brought in as point data. In order to reduce the effects of very high measurements on the regional heat flow, we set a maximum value of 120 mW/m² before contouring. The data were interpolated using EBK into a surface estimating heat flow across the region using the ArcGIS Geostatistical Wizard (Fig. 5). A surface estimating the standard error of the heat flow prediction was also created (Fig. 6). These surfaces were used as inputs in the script. The values from both of the surfaces were copied to the master point file. Normalized values served as the *evidence layer* data. The *confidence layer* was created by breaking up the standard error surface into five bins with each bin representing an equal portion of the standard error values between the minimum and maximum values. These bins were assigned a confidence value from a list in our script. Risk was calculated in the master point file by multiplying evidence by confidence.

2.3.3 Helium

Helium isotope data were cataloged as point locations using measured $^{3}He/^{4}He$ ratios relative to air (R/Ra) (*Dobson et al, 2015)*. Those values were used to weight a *simple density function* and create a density surface. Values from the density surface were copied to the master point file. Normalized values were used as the risk for helium.

2.3.4 Multicomponent equilibrium reservoir temperatures

Multicomponent geothermometer water temperatures *(Neupane et al., 2014)*, were contoured for prediction and standard error by the same means as the heat flow data before going into the script. Evidence values were calculated in the master point file using traditional normalization. Confidence values were assigned based on the standard error surface by the same process the heat flow data went through. Because it was decided that multicomponent equilibrium reservoir temperatures were not believed to have any relevance

beyond a particular distance, the last value in the list of confidence values was set to zero. Risk was calculated as the product of evidence and confidence. The zone with the lowest confidence therefore had zero values for risk.

2.3.5 Groundwater temperatures

Groundwater temperature data went through the exact same process as multicomponent geothermometer water temperatures. However the areas with lowest confidence were not set to zero because it was not assumed that their influence became irrelevant beyond a certain distance.

2.3.6 Heat Source CRS

The CRS values for *heat source* were calculated by multiplying each *element's* risk by its weight from the list of *intra-CRS weights* for *heat source* and then adding those products together and normalizing. These values represent the *heat source* CRS and were output to a raster surface (Fig. 7).

2.4 Seal

Two *elements* were examined in constructing the *seal* CRS map: lake sediments and aquifers. Both *data layers* were originally available as polygon files.

The lake sediment layer consisted of five polygons derived from regional geologic studies *(Desborough et al, 1989; Anderson et al, 1997; Wood et al, 2002; Cluer et al, 1986)*. Each was assigned a weight from a list of values as were areas with no lake sediments (Fig. 8-A). The distribution of a regionally extensive shallow aquifer in the eastern Snake River Plain *(Lindholm, 1996)* was used to establish either the presence or absence of an aquifer deemed deep enough to act as a *seal* and weights were established for both zones (Fig. 8-B). The product of these weight values became the CRS for *seal* (Fig. 8-C).

2.5 CCRS

The normalized CRS for *permeability* was multiplied by its *inter-CRS* value. This was added to the product of the normalized CRS for *heat source* and its *inter-CRS* value. This summed total was then multiplied by the CRS for *seal*. The normalized values are the data making up the CCRS.

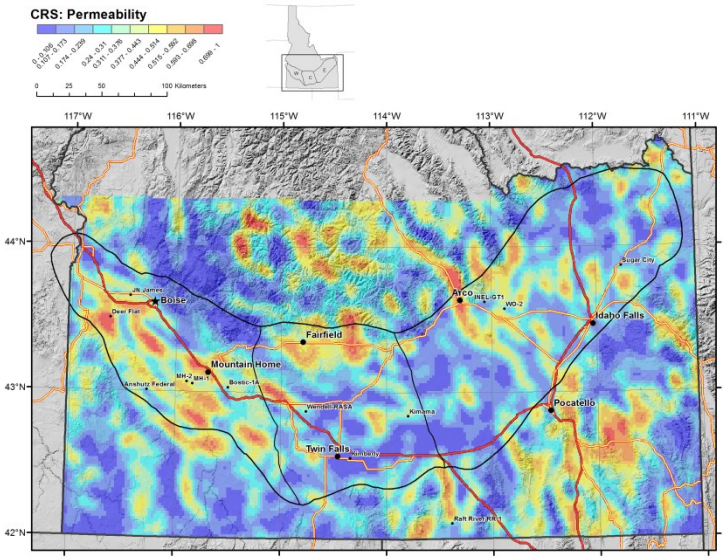

Figure 3. Common risk segment (CRS) map for Permeability: eight risk maps were weighted and combined to create the CRS map. Warm colors indicate regions with high favorability.

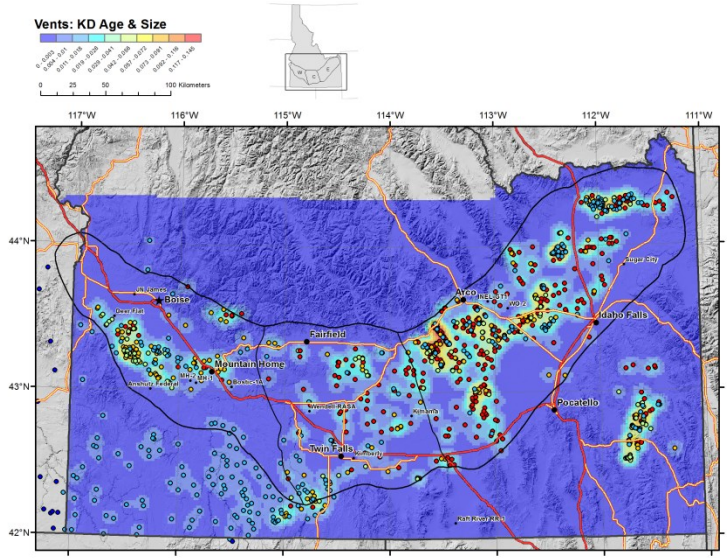

Figure 4. Kernel density surface of vents weighted by age and size. The product of the weights for age and size were used to weight the surface.

For both the *permeability* and *seal* CRS map, every *element* in each *component* was normalized and was weighted relative to the other *elements*. Data were normalized so that each *element's* influence would be of equal value prior to *intra-CRS weights* being applied. *Elements* were weighted relative to each other and summed. The summed values were normalized and became the CRS values. This was done so that the *inter-CRS weights* could be applied equally to the *components*. After each CRS was multiplied by its *inter-CRS weight*, these values were summed. This summed total was multiplied by values from the *seal* CRS map. This was done because our information for *seal* indicated that favorability for areas with a *seal* would be only slightly increased relative to the combined affect from *permeability* and *heat source*. Areas with no *seal* were weighted 0.81; areas with the greatest *seal* CRS values were weighted 1.0. The combined effect of *permeability* and *heat source* were reduced by a small amount in areas with less effect from *seal* because *seal* CRS values varied within a range of high values (0.81 – 1.0). CCRS values were calculated by normalizing those values in a new column of the master point file. Values were exported to raster surfaces for display. Areas with higher values reflect higher geothermal potential and are represented with warmer colors (Fig. 9). Areas of high geothermal favorability identified in the CCRS are highlighted in a companion paper at this meeting (*Shervais et al., 2016a*).

3. DISCUSSION

3.1 Description of Capabilities

The ability to automate processing and manipulate parameters has made it possible to refine our approach in creating a final CCRS map for assessing geothermal potential. Any parameter of any *element* in the study could be changed and the analysis could be run again. Values assigned to every *confidence layer* could be modified, as could weights for vent parameters, normalization values for heat flow, *intra-CRS weights*, and *inter-CRS weights*. Input layers could be substituted or modified. This made it possible to test assumptions, come up with a well-informed final product, and identify areas for further study.

In the second phase of this study, we plan to transfer these tools to smaller geographic areas identified in the CCRS as having high geothermal favorability using a finer resolution.

3.2 Possibilities for Future Work

In their current form, these tools are still built specifically for the data used in this study. Data from other studies could be processed with these tools; they would simply need to follow very strict conventions. In its current state, our program could easily be transferred, though different environments would require different layers and weights tailored to the conditions specific to that environment. We are presently working on improvements to the scripts to make them more easily transferrable to other studies and adapted for other users. Our goal is to turn the script into an ArcGIS Toolbox tool so that all of the tunable parameters available in the script could be made available as options in an interactive tool in ArcMap.

Our automated approach may eventually allow us to execute and evaluate a wide variety of weighting and input combinations in order to tune parameters more effectively. If other *knowledge-driven* weight combinations were proposed or *data-driven* weights were calculated, we could possibly execute and evaluate studies of those as well.

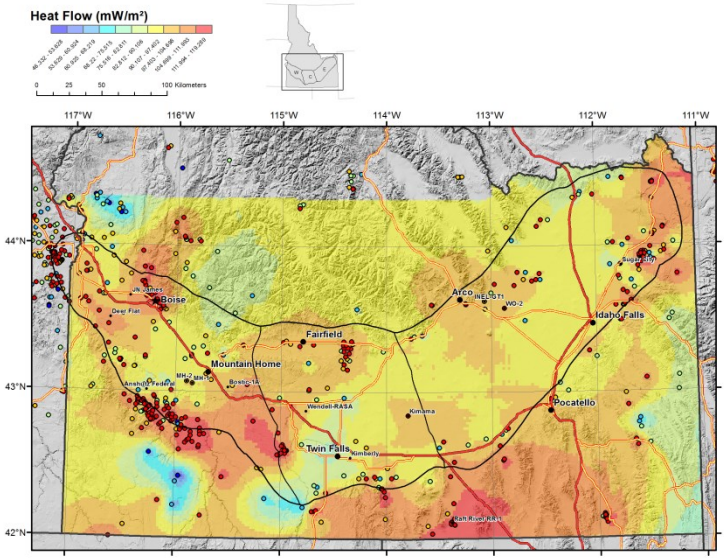

Figure 5. Heat Flow surface created using Empirical Bayesian Kriging from locations of measured heat flow showing estimated values of heat flow.

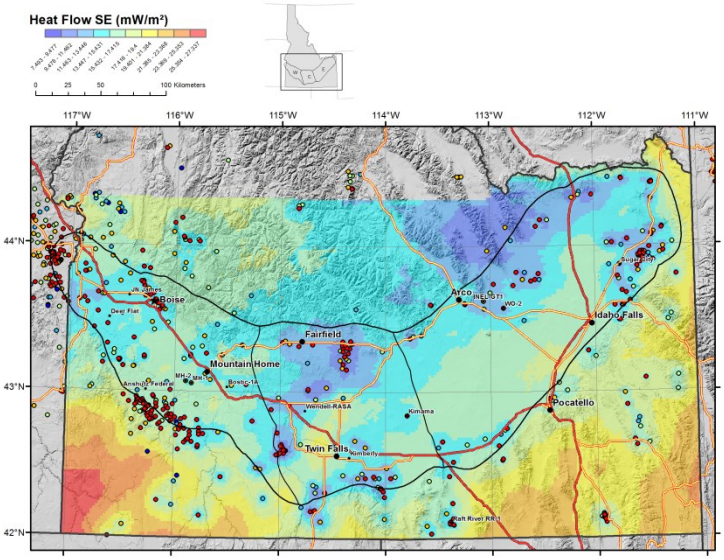

Figure 6. Heat flow standard error surface created using Empirical Bayesian Kriging from locations of measured heat flow showing the standard error of the predicted values of heat flow.

4.0 CONCLUSIONS

We have developed an approach to Play Fairway Analysis for use in geothermal exploration which is based on previously published conceptual models *(e.g., Nielson and Shervais, 2014; Nielson et al., 2015)* and builds on methods used in earlier GIS and evidence-based approaches in geothermal exploration *(e.g., Coolbaugh et al., 2002, 2005; Noorollahi et al., 2008; Trumpy et al., 2015)*. Most of the processing is automated by Python scripts that use ArcGIS tools as well as native Python capabilities. ArcMap is used to prepare input datasets for the script by conforming data to a common projection and by use of ArcMap Geostatistical Analyst to *interpolate* EBK surfaces.

All of the parameters that a user would want to modify in the study can changed either by editing lists or filepaths in the script or by modifying input *data layers*. The scripting automates hundreds of processing steps in its current configuration, rendering the process less prone to error, and allowing the user to rapidly test a variety of parameters, and assess parameter sensitivity. Our tools can be repeated, modified, scaled, and transferred to other settings.

Our approach has helped to identify areas of high geothermal favorability in the western and central Snake River Plain and will be used to further examine these smaller study areas at a finer scale and incorporate additional *elements* during the next phase of work (*Shervais et al., 2016*). By identifying favorable areas, this methodology helps to reduce uncertainty in geothermal energy exploration and development. The accessibility and flexible nature of the automated tools we have developed allow them to be easily modified to

accommodate new data or parameters. As a result, they are useful for all phases and scales of our study, and are easily transferable to other projects.

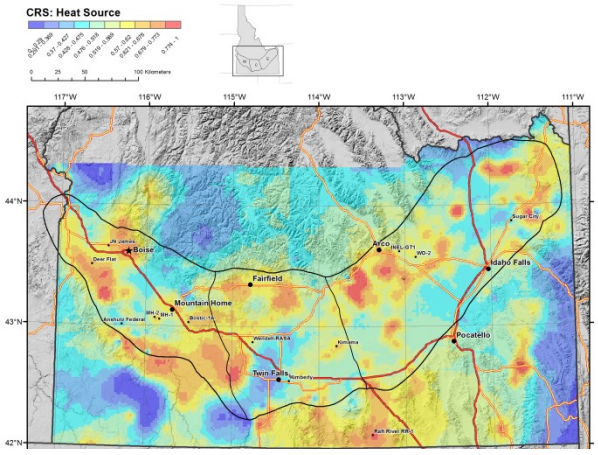

Figure 7. Common risk segment (CRS) map for Heat Source: five risk maps were weighted and combined to create the CRS map. Warm colors indicate regions with high favorability.

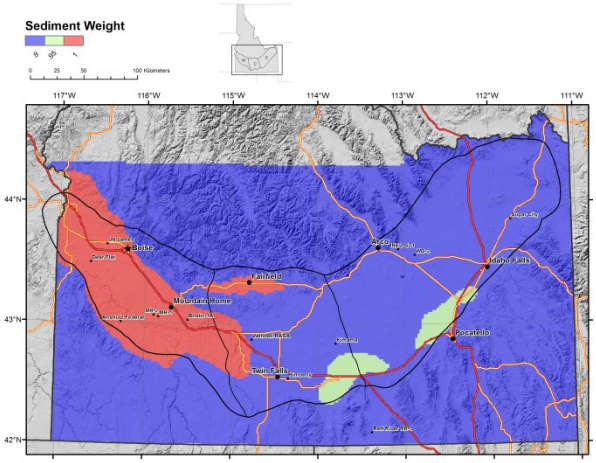

Figure 8-A. Weights for lacustrine lake sediments layer used in CRS map for Seal.

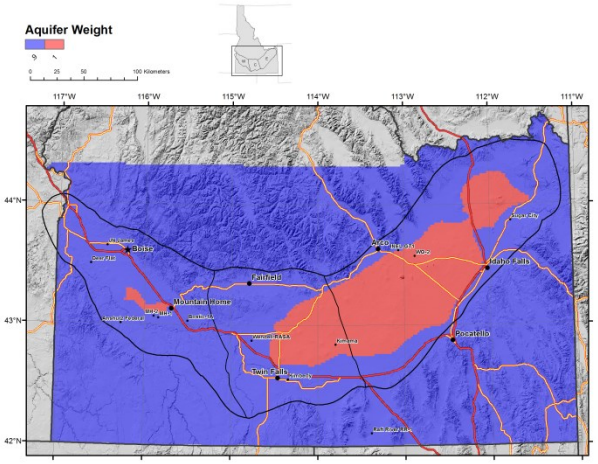

Figure 8-B. Weights for aquifer layer used in CRS map for Seal.

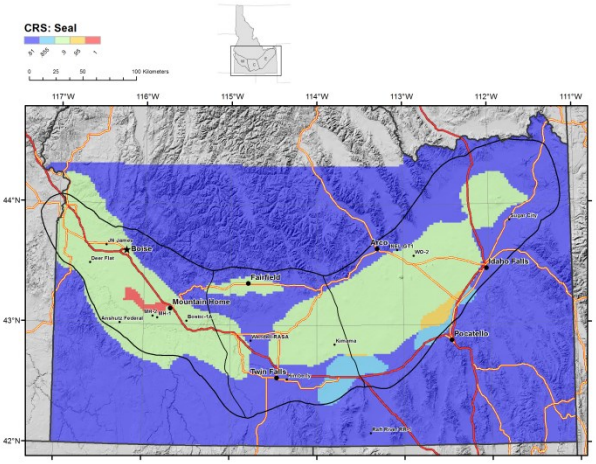

Figure 8-C. CRS map for Seal. Warm colors indicate regions with high favorability.

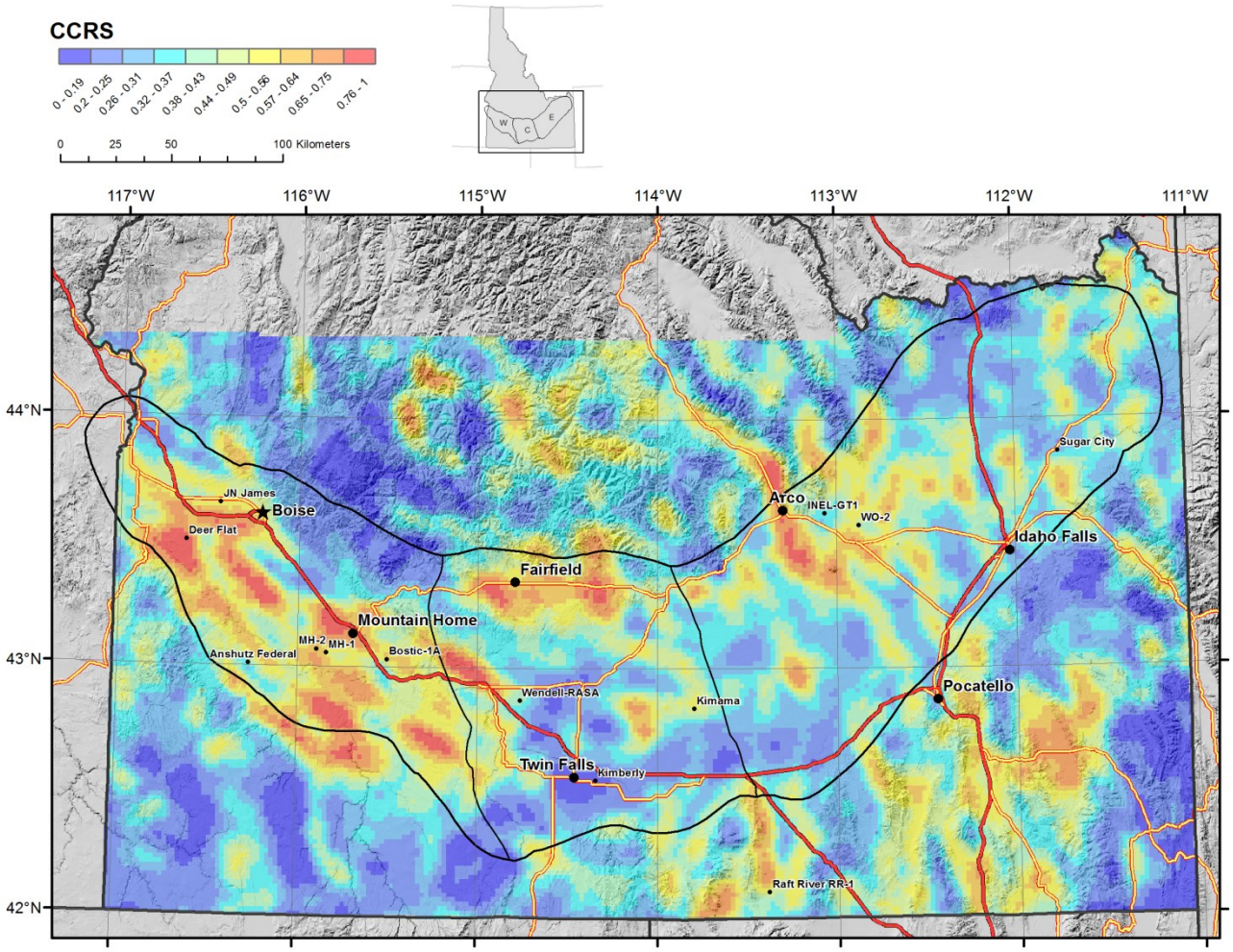

Figure 9. Composite Common Risk Segment (CCRS) map. Warm colors indicate regions with high geothermal favorability.

Acknowledgments

This work was supported by the U.S. Geological Survey Energy Resources Program, and by the U.S. Department of Energy Award EE-0006733. We wish to thank Colin Williams (U.S. Geological Survey) for guidance and discussions.

REFERENCES CITED

Anderson, S.R., Liszewski, M.J., and Cecil, L.D., 1997, Geologic ages and accumulation rates of basalt-flow groups and sedimentary interbeds at the Idaho National Engineering Laboratory, Idaho. USGS Water Resources Investigation Report 97-4010, 39 pp.

Bankey, V., Cuevas, A., Daniels, D., Finn, C.A., Hernandez, I., Hill, P., Kucks, R., Miles, W., Pilkington, M., Roberts, C., Roest, W., Rystrom, V., Shearer, S., Snyder, S., Sweeney, R., Velez, J., 1999, A New Magnetic Anomaly Map of North America, http://crustal.usgs.gov/projects/namad/the_project.html

Blackwell, D.D., 1989, Regional implications of heat flow of the Snake River Plain, northwestern United States: Tectonophysics, v. 164, p. 323-343.

Blackwell, D.D. and M. Richards, 2004, Geothermal Map of North America. Amer. Assoc. Petroleum Geologists, Tulsa, Oklahoma, 1 sheet, scale 1:6,500,000.

Bonham-Carter, G.F.: Geographic Information Systems for Geoscientists: Modeling with GIS, *Oxford: Pergamon Press*, (1994), p. 269.

Cluer, J.K. and Cluer, B.L., 1986, The late Cenozoic Camas Prairie Rift, south-central Idaho. Contributions to Geology, University of Wyoming, v24, 91-101.

Coolbaugh, M., Zehner, R., Kreemer, C., Blackwell, D.D., Oppliger, G.L., 2005, A map of geothermal potential for the Great Basin, USA: Recognition of multiple geothermal environments. Geothermal Resources Council Transactions, v. 29.

Coolbaugh, M., Zehner, R., Kreemer, C., Blackwell, D., Oppliger, G., Sawatzky, D., Blewitt, G., Pancha, A., Richards, M., Helm-Clark, C., Shevenell, L., Raines, G., Johnson, G., Minor, T., Boyd, T., 2005. Geothermal potential map of the Great Basin, western United States: Nevada. Bur. Mines Geol. Map (151).

Coolbaugh, M.F., Taranik, J.V., Raines, G.L., Shevenell, L.A., Sawatzky, D.L., Minor, T.B., Bedell, R., 2002, A geothermal GIS for Nevada: defining regional controls and favorable exploration terrains for extensional geothermal systems. Geothermal Resources Council Transactions v. 26, p. 485-490.

Desborough, GA, Raymond, W.H. Marvin, R.F. and Kellogg, K.S., 1989, Pleistocene sediments and basalts along the Snake River in the area between Blackfoot and Eagle Rock, southeastern Snake River Plain, southeastern Idaho. U.S. Geological Survey Open-File Report 89-436, 18 pp.

Dobson, P.F., Kennedy, B.M., Conrad, M.E., McLing, T., Mattson, E., Wood, T., Cannon, C., Spackman, R., van Soest, M., and Robertson, M., 2015, He isotopic evidence for undiscovered geothermal systems in the Snake River Plain. Proceedings, 40th Workshop on Geothermal Reservoir Engineering, Stanford University, Stanford, CA, 7 p.

Ferrill, D.A., Winterle, J., Wittmeyer, G., Sims, D., Colton, S., Armstrong, A., and Morris, A.P., 1999, Stressed rock strains groundwater at Yucca Mountain, Nevada: GSA Today, v. 9, no. 5, p. 1–8.

Glen, J.M., 2016, Gravity data, unpublished data.

Lindholm, G.F., 1996, Summary of the Snake River regional aquifer-system analysis in Idaho and eastern Oregon: U.S. Geological Survey Professional Paper 1408-A, 59 p.

Ludington, S., Moring, B.C., Miller, R.J., Evans, J.G., Stone, P.S., Bookstrom, A.A., Nutt, C.J., Bedford, D.R., Haxel, G.A., Hopkins, M.J., Flynn, K.S., 2005, Preliminary integrated geologic map databases for the United States - Western States - California, Nevada, Arizona, Washington, Oregon, Idaho, and Utah, http://pubs.usgs.gov/of/2005/1305/.

Machette, M.N., Haller, K.M., Dart, R.L., Rhea, S.B., 2003, Quaternary fault and fold database of the United States: U.S. Geological Survey Open-File Report 03-417, http://qfaults.cr.usgs.gov/faults/.

McCafferty, A.E., Kucks, R.P., Hill, P.L., Racey, S.D., 1999, Aeromagnetic Map For The State of Idaho, U.S. Geological Survey Open-File Report 99-371. http://pubs.usgs.gov/of/1999/ofr-99-0371/idaho.html

Morris, A., David, A.F., Henderson, B., 1996. Slip-tendency analysis and fault reactivation. Geology 24, 275–278.

Neupane, G., E.D. Mattson, T.L. McLing, C.D. Palmer, R.W. Smith, T.R. Wood, 2014, Deep Geothermal Reservoir Temperatures in the Eastern Snake River Plain, Idaho using Multicomponent Geothermometry. Proceedings, Thirty-Eighth Workshop on Geothermal Reservoir Engineering Stanford University, Stanford, California, February 24-26, 2014 SGP-TR-202.

Nielson, D.L. and Shervais, J.W., 2014, Conceptual model of Snake River Plain geothermal systems: Proceedings, Thirty-ninth Workshop Geothermal Reservoir Engineering, Stanford University, 2014), 1010-1016.

Nielson, D.L., J.W. Shervais, L. Liberty, S.K. Garg, J. Glen, C. Visser, P. Dobson, E. Gasperikova and E. Sonnenthal, 2015, Geothermal Play Fairway Analysis Of The Snake River Plain, Idaho. Proceedings Fortieth Workshop on Geothermal Reservoir Engineering, Stanford University, Stanford, California, January 26-28, 2015 SGP-TR-204.

Noorollahi, Y., Itoi, R., Fujii, H., Tanaka, T., 2008. GIS integration model for geothermal exploration and well siting. Geothermics 37, 107–131. doi:10.1016/j.geothermics.2007.12.001

Shervais, J.W., Evans, J.P., Glen, J.M., DeAngelo, J., Dobson, P., Gasperikova, E., Sonnenthal, E., Siler, D., Liberty, L.M., Visser, C., Nielson, D.L., Garg, S., Athens, N., Burns, E., Play Fairway Analysis of the Snake River Plain: Phase 1, *Proceedings,* 41st Workshop on Geothermal Reservoir Engineering, Stanford University, Stanford, CA (2016a). SGP-TR-209.

Shervais, J.W., Glen, J.M., Liberty, L.M., Dobson, P., Gasperikova, E., Sonnenthal, E., Visser, C., Nielson, D., Garg, S., Evans, J.P., Siler, D., DeAngelo, J., Athens, N., Burns, E., 2015, Snake River Plain Play Fairway Analysis - Phase 1 Report. Geothermal Resources Council Transactions, v. 39, 761-769.

Shervais, J.W., Evans, J.P., Glen, J.M., DeAngelo, J., Dobson, P., Gasperikova, E., Sonnenthal, E., Siler, D., Liberty, L.M., Visser, C., Nielson, D.L., Garg, S., Athens, N., Burns, E., 2016, Snake River Plain Play Fairway Analysis: Phase 1 Final Report, Report to Department of Energy Geothermal Technology Office, Project number DE-EE 0006733, January 2016b, 171 pp.

Shervais, J.W., Evans, J.P., Schmitt, D., Christiansen, E.H., and Prokopenko, A.A., 2014, HOTSPOT: The Snake River Scientific Drilling Project. EOS, Transactions American Geophysical Union; 95(10), 85-86. DOI:10.1002/2014EO100001.

Sibson, R.H., 1994. Crustal stress, faulting and fluid flow. Geological Society, London Special Publication, 78: 69-84.

Trumpy, E., Donato, A., Gianelli, G., Gola, G., Minissale, A., Montanari, D., Santilano, A., Manzella, A., 2015, Data integration and favourability maps for exploring geothermal systems in Sicily, southern Italy. Geothermics, Volume 56, Pages 1-16. doi:10.1016/j.geothermics.2015.03.004

Williams, C.F. and J. DeAngelo, 2008, Mapping Geothermal Potential in the Western United States. Geothermal Resources Council Transactions v. 32, 181-188.

DeAngelo, Shervais, Glen, Nielson, Garg, Dobson, Gasperikova, Sonnenthal, Visser, Lee, Siler, Evans, Santellanes

Williams, C.F., and J. DeAngelo, 2011, Evaluation of approaches and associated uncertainties in the estimation of temperatures in the upper crust of the western United States. Geothermal Resources Council Transactions, v. 35, 1599-1605.

Wood, S.H., Clemens, D.M., 2002, Geologic and tectonic history of the western Snake River Plain, Idaho and Oregon, in: Bonnichsen B., White C., and McCurry M., eds., Tectonic and magmatic evolution of the Snake River Plain volcanic province, Idaho Geological Survey Bulletin 30. Moscow, ID, United States. p. 69-103.

GLOSSARY

Common risk segment (CRS) map: Raster grid showing the magnitude of a *component's* significance. The CRS consists of the weighted sum of risk layers from a *component's elements*.

Component: General geologic factor contributing to favorability, comprised of *permeability*, *heat source*, and *seal*.

Composite common risk segment (CCRS) map: Raster grid showing the magnitude of the combined contributions of the study's CRS maps.

Confidence layer: Raster grid showing the magnitude of an *element's* uncertainty.

Data-driven: An approach to weighting *elements* that relies on statistical relationships.

Data layer: ArcGIS shapefile used in making an *evidence layer* for an *element*. *Data layers* are conformed to a common format.

Element: Geologic factor being modeled in *evidence*, *confidence* and *risk layers*.

Empirical Bayesian Kriging (EBK): An iterative geostatistical *interpolation* method.

Evidence layer: Raster grid showing the magnitude of an *element's* significance.

Heat Source: One of the three *components* used in the study comprised of the following *elements*: Heat flow, volcanic vents, helium isotopic ratios, multicomponent equilibrium reservoir temperatures, and groundwater temperatures.

Interpolation: Process of estimating a raster surface of continuous values from point locations.

Inter-CRS weights: Integer values that quantify the relative importance of *components* within the study.

Intra-CRS weights: Integer values that quantify the relative importance of *elements* within a *component*.

Kernel density function: Raster surface showing spatial density of point locations with the density distributed from a maximum value at the center to a zero value at the limit of the full radius using a quadratic function. These locations can be given weighted values.

Knowledge-driven: An approach to weighting *elements* that relies on expert opinion.

Permeability: One of the three *components* used in the study comprised of the following *elements*: Mapped faults, lineations interpreted from geophysics: mid-depth gravity, deep gravity, and magnetics.

Raw data: Original information obtained from the data's source used to create a *data layer* for an *element*.

Risk layer: Product of *evidence* and *confidence layers*; used in creating CRS map.

Seal: One of the three *components* used in the study comprised of the following *elements*: Lake sediments and aquifers.

Semivariogram: Function describing spatial correlation in measured point locations.

Simple density function: Raster grid showing spatial density of point locations. These locations can be given weighted values.